

Neural Computing and Applications

Explainable Machine Learning Inverse Problem Solution for EEG-based BCI

--Manuscript Draft--

Manuscript Number:	NCAA-D-20-01657
Full Title:	Explainable Machine Learning Inverse Problem Solution for EEG-based BCI
Article Type:	Original Article
Keywords:	Brain Computer Interface; Beamforming; Deep Learning; Explainable Machine Learning
Corresponding Author:	Cosimo Ieracitano Universita degli Studi Mediterranea di Reggio Calabria Reggio Calabria, ITALY
Corresponding Author Secondary Information:	
Corresponding Author's Institution:	Universita degli Studi Mediterranea di Reggio Calabria
Corresponding Author's Secondary Institution:	
First Author:	Cosimo Ieracitano
First Author Secondary Information:	
Order of Authors:	Cosimo Ieracitano Nadia Mammone Amir Hussain Francesco Carlo Morabito
Order of Authors Secondary Information:	
Funding Information:	
Abstract:	<p>Electroencephalographic (EEG) recordings can be of help in decoding the open/close hand's motion preparation. To this end, cortical source signals in the motor cortex (1s in advance with respect to the movement onset) are extracted by solving the inverse problem through beamforming. EEG sources epochs are used as sources-time maps input to a custom deep Convolutional Neural Network (CNN) that is trained to perform 2-ways classification tasks: pre-hand close (HC) vs. rest state (RE) and pre-hand open (HO) vs. RE. Although the deep CNN works well (accuracy rates up to 89.65+-5.29% for HC vs. RE and 90.50+-5.35% for HO vs. RE) in the present study we explore the interpretability of the deep CNN to provide further insights into the hidden activation mechanism of cortical sources during the preparation of hands' sub-movements. Specifically, an occlusion sensitivity analysis is carried out to investigate which cortical area is preferably involved in the classification procedure. Experimental results show a recurrent spatial pattern of cortical activation across subjects; in particular, the central region close to the longitudinal fissure and the right temporal zone of the premotor and the primary motor cortex. appear to be significantly involved. These findings encourage an in-depth study of cortical areas that seem to play a key role in hand's open/close preparation.</p>

[Click here to view linked References](#)

Noname manuscript No. (will be inserted by the editor)
--

Explainable Machine Learning Inverse Problem Solution for EEG-based BCI

Cosimo Ieracitano · Nadia Mammone ·
Amir Hussain · Francesco Carlo
Morabito

Received: date / Accepted: date

Abstract Electroencephalographic (EEG) recordings can be of help in decoding the open/close hand's motion preparation. To this end, cortical source signals in the motor cortex (1s in advance with respect to the movement onset) are extracted by solving the inverse problem through beamforming. EEG sources epochs are used as sources-time maps input to a custom deep Convolutional Neural Network (CNN) that is trained to perform 2-ways classification tasks: pre-hand close (HC) vs. rest state (RE) and pre-hand open (HO) vs. RE. Although the deep CNN works well (accuracy rates up to $89.65 \pm 5.29\%$ for HC vs. RE and $90.50 \pm 5.35\%$ for HO vs. RE) in the present study we explore the interpretability of the deep CNN to provide further insights into the hidden activation mechanism of cortical sources during the preparation of hands' sub-movements. Specifically, an *occlusion sensitivity analysis* is carried out to investigate which cortical area is preferably involved in the classification procedure. Experimental results show a recurrent spatial pattern of cortical activation across subjects; in particular, the central region close to the longitudinal fissure and the right temporal zone of the premotor and the primary motor cortex. appear to be significantly involved. These findings encourage

C. Ieracitano (Corresponding author)
DICEAM University Mediterranea of Reggio Calabria, Italy, Via Graziella Feo di Vito, 89124
E-mail: cosimo.ieracitano@unirc.it

N. Mammone
DICEAM University Mediterranea of Reggio Calabria, Italy, Via Graziella Feo di Vito, 89124
E-mail: nadia.mammone@unirc.it

A. Hussain
School of Computing, Edinburgh Napier University, Edinburgh EH10 5DT, Scotland, UK
E-mail: a.hussain@napier.ac.uk

F.C. Morabito
DICEAM University Mediterranea of Reggio Calabria, Italy, Via Graziella Feo di Vito, 89124
E-mail: morabito@unirc.it

1
2
3
4
5
6
7
8
9
10
11
12
13
14
15
16
17
18
19
20
21
22
23
24
25
26
27
28
29
30
31
32
33
34
35
36
37
38
39
40
41
42
43
44
45
46
47
48
49
50
51
52
53
54
55
56
57
58
59
60
61
62
63
64
65

1 an in-depth study of cortical areas that seem to play a key role in hand's
2 open/close preparation.
3

4 **Keywords** Brain Computer Interface · Beamforming · Deep Learning ·
5 Explainable Machine Learning
6

7 8 **1 Introduction** 9

10 Scalp lectroencephalography (EEG) is a non-invasive technique that collects
11 the electrical fields produced by the brain and reflects its underlying activ-
12 ity [34]. EEG is widely used as a basic diagnostics of several sneurological
13 diseases, and in neuroscience and cognitive research [6, 10, 18, 17]. EEG is com-
14 monly exploited in brain-computer interface systems (BCI), where the brain
15 directly communicates with an external device by decoding subject's inten-
16 tions from EEG signals and converting them in a set of suitable commands
17 [26]. EEG is relatively affordable, widely spread, easy to use, and generally
18 well tolerated by the patients. Unfortunately, it also has some non trivial limi-
19 tations: 1) a poor signal-to-noise ratio (SNR), and the brain's waves of interest
20 are usually corrupted by multiple sources of noise called *artifacts* [30]; 2) EEG
21 recordings are non-stationary signals, thus their statistical characteristics vary
22 across time [47]; 3) poor spatial resolution caused by volume conduction ef-
23 fects [28]; 4) high inter-subject variability that limits the ability of a classifier,
24 trained over a cohort of subjects, to generalize well across subjects [38]. One
25 of the greatest potentials of Deep Learning (DL) is the ability to generalize
26 even in presence of complex inputs [23]. In the context of the EEG analysis,
27 this would imply the possibility of identifying patterns relevant to classifica-
28 tion also in presence of additional non-target waves in the EEGs. However,
29 the main limitation in the application of DL to EEG processing lays in the
30 relatively small number of samples typically available in EEG databases, as
31 compared to the number of samples that can be found in computer vision or
32 natural language processing (NLP) applications, which made DL so powerful
33 in such fields. The following tasks have been mostly investigated so far by
34 applying DL to EEGs: motor imagery (MI) (22%), mental workload (16%),
35 emotion recognition (16%), seizure detection (14%), event related potential
36 detection (10%), sleep stage scoring (9%) and other studies (13%) [5]. MI is
37 task considered in the present study. BCI systems based on MI generally re-
38 quire the user to imagine performing a given movement in order to allow the
39 system to classify the imagined movement with good accuracy [27]. However,
40 sustained motor imagery is not natural neither comfortable for the user; in
41 addition, it requires intensive training and implies a delay between the onset
42 of imagination and the time the desired control is issued [32]. Conversely, in
43 motor preparation investigation, the subject performs or attempts to perform
44 the movement and the behavior of EEG signals before motion onset/attempt
45 is investigated to predict the intended movement [43]. Decoding the prepara-
46 tion of the movement, whether it is actually implemented or just attempted
47 (in case the subject has a motor disability hindering motor implementation),
48
49
50
51
52
53
54
55
56
57
58
59
60
61
62
63
64
65

1 would be much more natural and immediately decodable [36]. Furthermore,
2 the mechanisms of motor preparation are not clear. Previous studies showed
3 that premotor cortex is activated contralaterally during motor preparation,
4 which was observed by fMRI/NIRS and also in EEG signals [45], however it
5 is not clear if and how the different sub-areas of premotor cortex work to-
6 gether to develop motion planning. For the aforementioned reasons, in [29]
7 motor preparation of different sub-movements of upper limbs was investigated
8 by analyzing frames of EEG signals preceding motion's onset and by compar-
9 ing them with frames of EEGs collected in absence of any motion planning
10 (resting). Mammone et al. [29] reached an accuracy of $90.30 \pm 5.6\%$ in pre-
11 movement vs. resting discrimination and of $62.47 \pm 6.7\%$ in the discrimination
12 of the preparation of different sub-movements. A deep Convolutional Neural
13 Network (CNN) was designed and trained through stratified time-frequency
14 maps of 210 EEG source locations in the premotor and primary motor cor-
15 tex. However, no interpretation of the results was provided, as artificial neural
16 networks act as a black-box. Furthermore, training a deep CNN over mul-
17 tichannel images (time, sources and frequency) requires the adaptation of a
18 very large number of parameters and hence would require a large database to
19 be trained. In the present work, we aim at achieving good accuracy in motor
20 planning classification of hands' movements by designing a deep CNN to be
21 trained over single channel images (time vs. sources). In the present work,
22 explainable machine learning (EML) is proposed to investigate motor prepara-
23 tion by exploring the behavior of the trained network [31]. In summary, the
24 aim of the present work is twofold: 1) To design a novel deep CNN that, by
25 processing EEG source signals of the motor cortex, is able to discriminate
26 the phases of preparation of hands' movements (open/close) from resting (no
27 movement planning); 2) To explain the achieved results by means of EML,
28 in order to assess which EEG sources (i.e., which cortical locations) play a
29 decisive role in the classification of hand's motor preparation phases. The final
30 aim is to find out possible areas in the motor cortex that are mainly involved
31 in planning hands' movements. In fact, while it is well known which areas are
32 most involved in the implementation of movements of the different parts of
33 the body [4], because the activation of the movement is triggered by relatively
34 well localized areas in the primary motor cortex, it is not well known how
35 motor planning is spatially organized. EML could yield a significant contri-
36 bution in this field [8]. To this end, a deep CNN was designed and trained to
37 discriminate hand's opening (HO) and hand's closing (HC) motion prepara-
38 tion phases from resting (RE) phases. The training database was constructed
39 by processing EEG signals collected from 15 subjects recruited within a BCI
40 study conducted by Ofner et al. [35]. The paradigm followed in [35] provided
41 that the subject performed cue-based movements starting from a neutral rest
42 position. The present analysis is focused on the classification of HC vs. RE and
43 HO vs. RE. The developed CNN receives as input the electrical activity of 210
44 sources located in the motor cortex in the time interval of 1 s preceding mo-
45 tion onset. Such source signals were estimated by solving the inverse problem
46 starting from EEG scalp signals. The developed CNN was able to discriminate
47
48
49
50
51
52
53
54
55
56
57
58
59
60
61
62
63
64
65

premov (HC or HO) vs RE with an average accuracy of 90%. An occlusion sensitivity analysis was subsequently carried out by passing the time-source maps as input to the network to find out which sources (i.e., cortical locations) are estimated to be more relevant in the classification of HC/HO from RE. We could observe a recurrent spatial pattern across subjects that show greater activation of the left part of the motor cortex in the central area, close to the longitudinal fissures between the two hemispheres, together with the extreme right part of the motor cortex belonging to the temporal lobe.

The paper is organized as follows: in Section 2 the proposed method is presented. The preprocessing steps including beamforming technique and cortical sources extraction are also described. Section 3 shows the proposed deep CNN for the pre-movements tasks classification, whereas, Section 4 introduces the salient cortical source recovery procedure by means of EML (i.e. occlusion sensitivity analysis). In Section 5 experimental results are reported. Section 6 discusses the achieved findings and Section 7 concludes the paper.

2 Methodology

The proposed methodology is shown in Figure 1; it includes the following processing modules:

1. *Extraction of premotor EEG epochs*: EEG segments preceding the (open/close) movements of the right hand as well as the rest condition are extracted from the available EEG dataset.
2. *Inverse problem solution and extraction of the cortical EEG sources*: beamforming technique is applied to reconstruct EEG sources corresponding to a given EEG epoch. It is worth noting that among the 2000 cortical locations of the adopted head model, those related to the areas 4 and 6 of Brodmann (i.e., the primary motor and the premotor cortex) are considered. Specifically, 210 EEG sources are extracted.
3. *DL-based system for pre-movements tasks classification*: the extracted 210-EEG sources are fed into a DL-based classifier. Specifically, a deep CNN is developed to perform the following binaries classifications: HC vs. RE and HO vs. HO. The deep CNN receives time-source maps as input (matrices sized 210 x 512, where 210 are the source locations under consideration and 512 is the sampling rate).
4. *Explainable DL system, salient cortical source recovery*: occlusion sensitivity analysis is applied to investigate which cortical area are more relevant to the open/close hand motion planning. Specifically, portions of the input maps (i.e., time-source maps) are occluded with the aim of detecting the cortical area that mostly affected the classification. K-means clustering technique is then used to segment the saliency maps and automatically detect the cortical source locations most relevant to the task prediction.

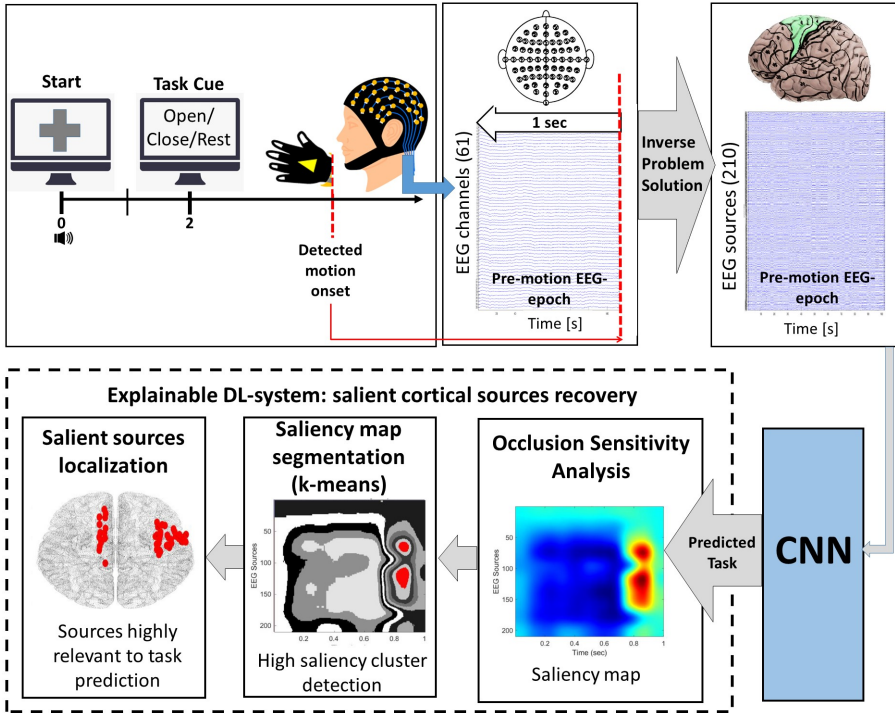


Fig. 1 Flowchart of the proposed framework. The subject is initially in a rest condition watching a monitor in front of him/her. After a beep (at 0 s), a fixation cross is produced on the monitor in order to make him/her focus his/her attention on it. Next (at 2 s), the cue of the desired task (i.e., HC/HO) is shown. The subject performs the cued movement and then returns to the original neutral position. The temporal window of 1s preceding motion execution (i.e., pre-motion EEG epoch) is extracted and the inverse problem is solved by means of beamforming technique in order to reconstruct the EEG sources. Notably, 210-EEG cortical sources (i.e., pre-motion EEG sources epoch) belonging to the motor cortex are taken into account and used as input to a customized deep CNN which is trained to perform the following binary classification tasks: HC vs. RE and HO vs. RE. Finally, an occlusion sensitivity analysis is carried out to detect the most significant regions in the input map (i.e., epoch of the EEG signals) involved in the classification process. The achieved saliency map is then segmented by k -means clustering and the cluster associated to highest saliency is identified. Sources belonging to that cluster interpreted as providing the largest contribution in decoding the specific movement.

2.1 Extraction of premotor EEG epochs

In the present research, a publicly available database of EEG recordings co-registered with signals collected from motion sensors [35] was used to construct the training and testing dataset. The database can be found at <http://bnci-horizon-2020.eu/database/data-sets> together with detailed information about channel layout, recording settings and paradigm description. The study involved 15 healthy subjects (aged 27 ± 5 years, nine of them are females). EEG signals were acquired by Ofner et al. [35] by means of 61 ac-

1 tive EEG electrodes and four 16-channel amplifiers (g.tec medical engineering
2 GmbH, Austria). Right mastoid channel was used as reference one and AFz
3 was set as ground channel. EEG signals were band-pass filtered between 0.01
4 Hz and 200 Hz (8-th Chebyshev filter), notch filtered at 50 Hz and sampled
5 at 512 Hz. The database consists of a motor execution and a motor imagery
6 part. Since the goal of the present study was to investigate motor preparation,
7 the first part was included in the analysis. During the experiment, subjects
8 remained seated on a comfortable chair and an anti-gravity exoskeleton (Ho-
9 coma, Switzerland) supported their right arm. The paradigm consisted in ex-
10 ecuting cue-based movements of the right upper limb starting from a neutral
11 position (lower arm extended to 120 degree and in a neutral rotation, hand
12 half open) [35]. The experiment consisted of 10 runs, every run included 6
13 trials and every trial included one hand open (HO), one hand close (HC) and
14 one rest (RE) cues. The timeline of the paradigm can be summarized as fol-
15 lows: At second 0, a fixation cross appeared on a computer screen, positioned
16 in front of the subject, to attract her/his gaze on it and limit eye movements.
17 At second 2, the cue of the task to be performed (HC/HO/RE) appeared on
18 the computer screen. After task execution, the subject moved her/his hand
19 back to the starting neutral position. In order to train a neural network to
20 decode motor preparation phases from EEG signals, a dataset of EEG epochs
21 preceding motion onset was necessary. To this purpose, the onset of movement
22 was estimated by processing motion data collected by glove sensors. Specifi-
23 cally, the onset of movement was detected by processing the signals recorded
24 from motion sensors embedded in the glove, following the procedure described
25 in [35]. The marked onset timing was manually checked for all of the 1800
26 pre-motion epochs under examination and the frames (epochs) of EEG sig-
27 nals preceding the marked onset were extracted accordingly. Such epochs were
28 included in the analysis together with a balanced set of resting EEG epochs.
29 Specifically, 900 EEG epochs (derived from 10 runs x 6 trials x 15 subjects)
30 per movement class (hand open/hand close) were taken into account. In order
31 to generate a balanced dataset, a comparable number of resting state EEG
32 epochs was extracted. In the end, 2700 EEG epochs (derived from 10 runs
33 x 6 trials x 15 subjects 3 classes) were extracted from the EEG recordings
34 and included in the dataset. As regards the choice of the length of the frame
35 preceding motion onset, it was set at 1 s after taking into account the typical
36 timeline of motor related cortical potentials (MRCP) which are brain waves
37 that arise together with movements' preparation and initiation [40,29].
38
39
40
41
42

43 2.2 Inverse problem solution and extraction of the cortical EEG sources

44 It is known that the EEG has a very good temporal resolution but a poor spa-
45 tial resolution, due to volume conduction effects [34,11,13]. Inverse problem
46 solution is a possible way to deal with such effects. In the proposed method-
47 ology, EEG signals are used to reconstruct a set of source signals where every
48 source signal represents the contribution of a source location (current dipole)
49
50
51
52
53
54
55
56
57
58
59
60
61
62
63
64
65

located in the cortex [11,13]. Solving the “inverse problem” means reconstructing source locations’ contribution to the overall EEG signals collected at the scalp. EEGs can be hypothesized to be the projection of sources’ contributions from cortical locations to scalp sensors through a “forward model” [7]. Such forward model takes into account the structural and conductive properties of brain tissues. In the frequency range of EEG signals, the quasi-static approximation of Maxwell’s equations can be assumed hence the forward model becomes linear [14] and be formulated as follows:

$$\mathbf{x}(t) = \mathbf{L}\mathbf{q}_r(t) \quad (1)$$

$\mathbf{q}_r(t)$ is the 3 dimensional directed current dipole associated to cortical location “ r ” (where $r=1,\dots,N_s$ and N_s is the number of possible source locations in the cortex); \mathbf{L} is known as “lead field” matrix, which represents the head model that projects the current dipole $\mathbf{q}_r(t)$ into the scalp potential $\mathbf{x}(t)$ [14]. The number of sources N_s is typically larger than the number of channels N_c thus estimating $\mathbf{q}_r(t)$ from $\mathbf{x}(t)$ is inherently an ill posed problem. The adopted head model consists of 2000 cortical locations ($N_s=2000$) whereas the number of scalp channels of the EEG recordings analysed in the present work is $N_c=61$. In this work, the *New York Head* (NYH) forward model, developed by Haufe et al. [15], was adopted. Such head model is based on the popular ICBM152 anatomy, a nonlinear average of T1-weighted structural MR images collected from 152 adults. By solving the inverse problem, cortical current dipoles $\mathbf{q}_r(t)$ are estimated starting from the recorded EEG signals $\mathbf{x}(t)$ and from the lead field matrix \mathbf{L} . Several inverse problem solution approaches can be found in the literature on EEG source imaging: minimum-norm solutions, beamformers, and dipole modeling [11,41]. Beamforming solves the inverse problem by maximizing the contribution of a given source location while suppressing contributions from the other ones and was proved very effective in BCI applications by Grosse-Wentrup et al. [12]. The premotor and primary motor cortex are considered crucial in movement planning and execution [16, 19]. Such regions fall in the Brodmann’s Areas 4 and 6 of the brain [3]. Each one of the 2000 available source locations was associated to the corresponding Brodmann Area through its Montreal Neurological Institute (MNI) stereotaxic coordinates. MNI coordinates of every source locations were known. First of all, they were indeed converted into Talairach coordinates [22] and then matched with Talairach Atlas labels [1], in order to come up with the corresponding Brodmann area of every source location. In the end, 210 locations belonging to Brodmann areas 4 and 6 were selected out of the 2000 available ones.

3 Deep Learning-based system for pre-movements tasks classification

A deep learning classifier is proposed to discriminate EEG source epochs belonging to the pre-movement (close/open) of the right hand (HC/HO) or to the resting state (RE) class. Notably, a deep Convolutional Neural Network

(CNN) is developed to perform the 2-ways classification tasks: the HC vs. RE and HO vs. RE.

3.1 Convolutional Neural Network

CNN is a well-known deep learning model widely used especially in computer vision [25,42] and image recognition [9,24]. It is composed of subsequence layers of *convolution*, *activation*, *pooling* followed by a multi-layer fully conneted neural network for classification purpose [21]. The *convolutional* layer includes a bank of J filters used to estimate the dot product (i.e., covolution operation) with the input map \mathbf{T} sized $t_1 \times t_2$. More specifically, each filter (sized $j_1 \times j_2$) performs the convolution with the selected local area and sweeps over the input representation with a specific stride using the same values of weights. This operation results in the so called *features maps* \mathbf{Z} of size $z_1 \times z_2$:

$$z_1 = \frac{t_1 - j_1 + 2 \times p}{s} + 1 \quad (2)$$

and

$$z_2 = \frac{t_2 - j_2 + 2 \times p}{s} + 1 \quad (3)$$

where p is the zero padding parameter. The *activation* layer introduces nonlinearity in the model. Specifically, here, the *Rectified Linear Unit* (ReLU) is employed for its ability to achieve good generalization and training time [33]. The *pooling* performs a downsampling operation of the feature maps resulting from the previous layer. The max pooling operation is used for its good translation-invariant properties [39]. It has a filter sized $\bar{j}_1 \times \bar{j}_2$ that scans the input feature map with stride \bar{s} . This operation outputs a reduced map sized $\bar{t}_1 \times \bar{t}_2$, with:

$$\bar{r}_1 = \frac{t_1 - \bar{j}_1}{\bar{s}} + 1 \quad (4)$$

and

$$\bar{r}_2 = \frac{t_2 - \bar{j}_2}{\bar{s}} + 1 \quad (5)$$

The CNN ends with a standard feed-forward MLP composed of a softmax output function used for discriminations tasks.

3.2 Design of the deep CNN

The proposed CNN is developed to accept as input time-source maps (i.e., EEG sources epochs) sized $t_1 \times t_2$, where $t_1=210$ represents the number of sources taken into account in this study, and $t_2=512$ represents the number of samples included in 1s temporal epoch before the movement onset. The

1 deep learning model consists of three stacked modules of convolutional ($conv_i$,
 2 with $i=1,2,3$), ReLU and max pooling ($mpool_i$) layers followed by a common
 3 MLP for performing the 2-ways classification: HC vs. RE and HO vs. RE.
 4 Figure 2 shows the architecture of the proposed deep CNN. Note that the
 5 topology of the developed model was set-up after several tests and using a
 6 *trial-and-error* strategy. Specifically, the temporal data (210 x 512) are firstly
 7 convolved with 4 learnable filters sized 5 x 5 ($conv_1$). Every filter scans the
 8 input representation with stride 1 resulting in 4 feature maps sized 206 x 508
 9 (according eq. 2, with $p=0$). After applying the ReLU activation function,
 10 max pooling is used to squeeze the input space from 206 x 508 to 68 x 169
 11 ($mpool_1$). This layer has the filter size 5 x 4 and stride equal to 3. Next, the four
 12 features maps extracted from $mpool_1$ are fed into a new layer of convolution
 13 ($conv_2$) composed of 8 filters sized 5 x 5 and unit stride, producing 8 maps
 14 of dimension 64 x 165 to which the ReLU activation function is applied. The
 15 second max pooling layer ($mpool_2$) has filter size 4 x 6, stride=3 and outputs
 16 8 downsampled representation of size 21 x 54. Similarly, the last convolutional
 17 layer ($conv_3$) has 16 filters sized 5 x 5 and unit stride. The resulting features
 18 maps have dimension of 17 x 50. Finally, the ReLU activation function is
 19 applied and the third max pooling layer ($mpool_3$) generates 16 maps sized 5
 20 x 16 (filter size 5 x 5, stride 3). The flatten vector of dimension 5 x 16 x 16 =
 21 1280 inputs a standard 2-hidden layers MLP consisted of 500 and 50 hidden
 22 units respectively, employed to perform the binaries classifications: HC vs. RE
 23 and HO vs. RE.
 24
 25
 26
 27
 28
 29
 30
 31
 32
 33
 34
 35
 36
 37
 38
 39
 40
 41
 42
 43
 44
 45
 46
 47
 48
 49
 50
 51
 52
 53
 54
 55
 56
 57
 58
 59
 60
 61
 62
 63
 64
 65

3.3 Learning parameters set-up

37 The Adaptive Moment (Adam) optimization procedure [20] was used to train
 38 the proposed deep CNN (Figure 2), using mini-batches size of 28. Training
 39 options were set-up by using the practical recommendations reported in [2,20],
 40 specifically: learning rate $\alpha=10^{-2}$, first moment decay rate $\beta_1=0.9$, and second
 41 moment decay rate $\beta_2=0.999$. The network was implemented with MATLAB
 42 R2019a and trained over about 50 iterations on two Nvidia GeForce RTX
 43 2080 Ti GPU, each with 11 GB memory, installed on a processor Intel(R)
 44 Core(TM) i7-8000K CPU @ 3.70GHz and RAM of 64 GB. Furthermore, the
 45 proposed deep CNN was trained and tested iteratively by using epochs of the
 46 each subject under analysis. Thus, 15 CNN classifiers were trained and tested.
 47 The estimated training time was of about 10 min per subject (applying the
 48 k -folds cross validation procedure, with $k=10$).
 49
 50
 51
 52
 53
 54
 55
 56
 57
 58
 59
 60
 61
 62
 63
 64
 65

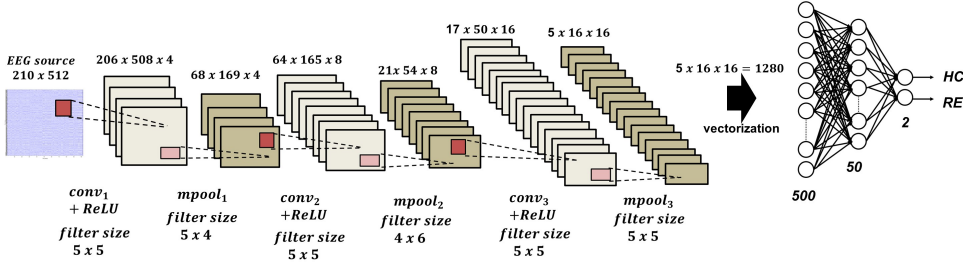


Fig. 2 Architecture of the proposed deep CNN. It consists of three convolutional layers (followed by ReLU non-linearity) and three max pooling layers. The network ends with a 2-hidden layers MLP employed to perform the 2-ways classifications: HC vs. RE and HO vs. RE.

4 Explainable Deep Learning system: salient cortical source recovery

4.1 Occlusion sensitivity analysis

Occlusion analysis has been widely used in image classification to show the sensitivity of a pre-trained CNN to different areas of an input image [46]. It consists in systematically occluding different patches of the input data with a grey mask and estimating the related effect on the network output. For each mask location the discrimination is performed using a pre-trained CNN and estimating the change in classification score for a specific class than the initial prediction (input without occlusion). Such changes in classification result in the so called *heatmap* or *saliency map* \mathbf{H} with a coloration ranging from blue to red and with the same input dimension. This representation reveals which area of the image is the most essential for the classification. Specifically, red color corresponds to higher values and consequently represent the most significant area that contributed to identify the specified class. When this region is occluded the classification performance decreases. Blue color corresponds to lower values and represents the areas not relevant during the discrimination task. In this study, the occlusion technique is applied to recover the cortical sources that are activated during the (open/close) hand's movement preparation. Given a subject under analysis, the e^{th} EEG source epoch (sized 210 x 512) is repeatedly occluded with a 42 x 256 pixel grey mask that moves across the input data with a vertical and horizontal stride of 21 and 51, respectively. It is worth noting that the dimension and stride of the mask has been set-up empirically, after several experiments. For each position of the mask, the 2-way discrimination task (i.e., HC vs. RE or HO vs. RE) is performed by using the proposed pre-trained CNN (Sect. 3.2). The output is a heatmap sized 210 x 512. As an example, Figure 3a shows the input map (i.e., EEG sources epoch) when a portion is occluded by a grey mask; whereas, Figure 3b

reports the achieved saliency representation map. In this case, as can be seen the red area, roughly corresponding to the sources ranged between (130-180) and in the temporal window (0.7-0.9), denotes the most relevant zone in the classification process. Further considerations and analyses are reported in the Experimental Results Sect. 5.2.

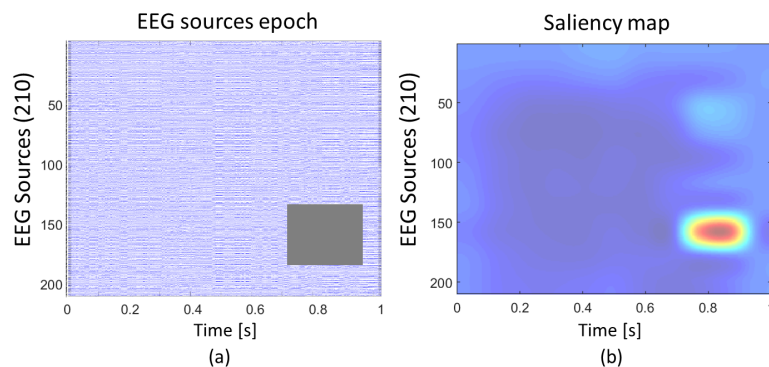


Fig. 3 (a) EEG sources epoch when a sub-region is occluded by a grey mask, that slides along the whole input size. (b) Saliency map with a coloration ranging from blue to red. Blue color represents low values that correspond to regions not significant for the classification task, vice-versa, red color represents high values that correspond to regions significant for the specified discrimination class.

4.2 Saliency maps segmentation through k-means

In order to provide a deeper understanding of which sub-areas in the motor cortex gave the largest contribution to decode movements' planning, a segmentation of the saliency maps was necessary in order to extract the high saliency zones automatically. To this end, the k -means clustering algorithm was applied to partition each saliency map to $k=10$ clusters. K -means is a widely applied clustering algorithm [44]. Its aim is to gather data points into a given number of clusters by following an iterative four-steps procedure:

1. the initial cluster centers are set randomly;
2. data points are assigned to the nearest cluster by estimating the euclidean distance between the data point and the cluster centers, in this way clusters are redefined;
3. update the clusters' centers;
4. go back to step 2. and repeat the procedure from 2. to 4. until the cluster centers do not change or the specified iteration number is reached.

After applying k -means to the saliency maps, the cluster associated to the highest saliency values was detected, the corresponding highly salient sources were extracted and mapped onto the cortex by red dots.

5 Experimental Results

5.1 Classification performance of the pre-movements tasks

The classification performance of the proposed deep CNN were evaluated using standard metrics (accuracy, recall, precision, F1-score):

$$Accuracy = \frac{TP + TN}{TP + TN + FP + FN} \quad (6)$$

$$Recall = \frac{TP}{TP + FN} \quad (7)$$

$$Precision = \frac{TP}{TP + FP} \quad (8)$$

$$F1 - score = 2 \times \frac{Precision \times Recall}{Precision + Recall} \quad (9)$$

where TP and TN are true positive and negative, respectively; whereas, FP and FN are false positive and negative, respectively [37]. Notably, TP is the number of EEG sources epochs belonging to HC/HO category and correctly classified as HC/HO; TN is the number of EEG sources epochs belonging to RE category and correctly classified as RE; FP is the number of EEG sources epochs belonging to RE misclassified as HC/HO and vice-versa FN are EEG epochs of HC/HO class erroneously identified as RE. In this study, 15 CNNs were trained and tested, 1 per subject, and the following 2-ways discrimination tasks were performed: HC vs. RE and HO vs. RE. The dataset of each binary classifier was composed of 120 EEG epochs (i.e., 60 belonging to HC/HO and 60 to RE). The k -fold cross validation technique was applied (with $k=10$), in particular: the train set included 70% of data (i.e. EEG sources epochs) and the test set the remaining 30%.

Table 1 reports results of the HC vs. RE classification. Remarkable discrimination values were observed in all subjects, reporting average recall, precision, F1-score and accuracy of $89.14 \pm 7.24\%$ and $91.19 \pm 7.88\%$, $89.69 \pm 4.98\%$, $89.65 \pm 5.29\%$, respectively. It is worth noting that the highest individual classification performance was achieved by Sb_{08} with accuracy of $98.02 \pm 2.10\%$, F1-score of $97.94 \pm 2.21\%$, recall of $96.03 \pm 4.20\%$ and precision of 100%; while the lowest individual classification performance was achieved by Sb_{07} . However, also in this case high discrimination scores were observed, but with higher standard variation: accuracy of $79.76 \pm 10.11\%$, F-score of $79.86 \pm 9.60\%$, recall of $80.16 \pm 12.77\%$ and precision of $80.83 \pm 12.36\%$

Table 2 reports results of the HO vs. RE classification. Also in this scenario very good performance were observed (average recall of $89.31 \pm 8.02\%$, average precision of $93.04 \pm 7.66\%$, average F1-score of $90.41 \pm 5.32\%$ and average accuracy of $90.50 \pm 5.35\%$). Notably, Sb_{08} and Sb_{02} achieved the best performances in terms of accuracy and F1-score; while, Sb_{07} reported the worst individual classification performance with an accuracy value of $75.79 \pm 9.72\%$ and F1-score of $76.95 \pm 5.87\%$.

5.2 Salient cortical source locations recovery

Occlusion sensitivity analysis was performed by using the proposed pre-trained deep CNN to estimate the saliency of each one of the 210 EEG sources. Specifically, for each subject, an averaged saliency map was estimated by averaging the saliency maps corresponding to the HC/HO EEG epochs correctly classified during the testing procedure and herein denoted as $\tilde{\mathbf{H}}_{Sb_i}^{tk}$, where tk represents the pre-movement task (i.e., HC/HO) and Sb_i is the subject under analysis (with $i=1,2,..15$). As an example, Figure 4a illustrates the average saliency map of Subject 08 while preparing to perform hand closing ($\tilde{\mathbf{H}}_{Sb_{08}}^{HC}$). Saliency is encoded with a coloration going from blu (low saliency) to red (high saliency). Highly salient EEG source locations can be recovered by detecting the EEG sources associated to red areas in the saliency map. Notably, red areas denote that the classification score decreases when the corresponding local regions of the input were hidden by the mask, which means that the occluded area is relevant to classification. In the example map shown in Figure 4a, the area located around 0.85s and approximately associated to the EEG sources ranging from 70 to 170, looks colored in red hence it resulted relevant to the decision making. Average saliency maps were then segmented as described in Sect. 4.2. Figure 4b depicts the clustered saliency map of Subject 08. Notably, the red area represents the cluster with the highest saliency and refers to the most relevant EEG sources, which were then mapped onto the cortex (red dots in Figure 4c). In the example shown in Figure 4c), EEG sources located in the left central zone (close to the longitudinal fissure) and in the right-temporal zone contributed the most to decoding hand closing motor planning. Following the aforementioned procedure, salient source locations in HC and HO motor preparation were estimated for every subject and are shown in Figure 5. It is worth to note the a recurrent spatial pattern of cortical activation (left central zone close to the longitudinal fissure and right-temporal zone) which occurred similarly during HC or HO motor preparation. Such pattern occurred in 10 out of 15 subjects during hand closing preparation and in 11 out of 15 subject in hand opening preparation. Nine out of 15 subjects exhibited the same spatial pattern in HC as well as in HO motor planning.

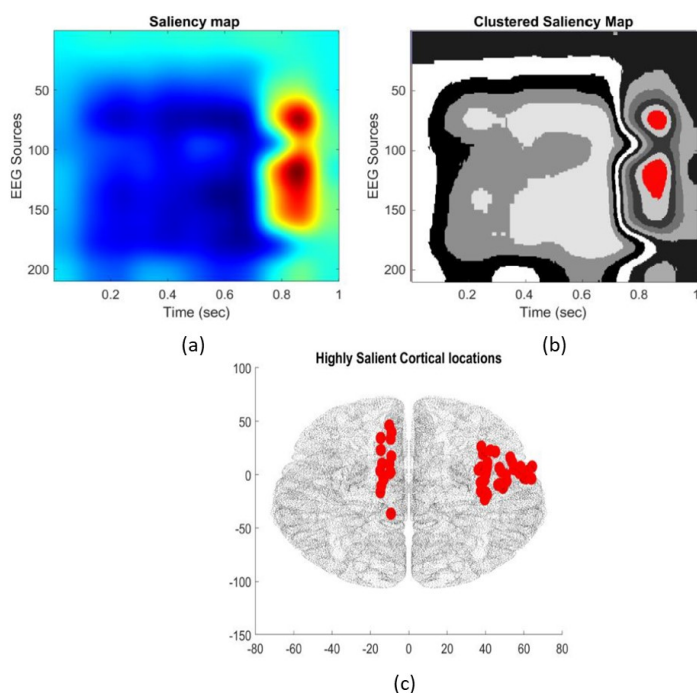


Fig. 4 (a) Saliency map of Subject 08 while planning to perform HC task, achieved by occlusion sensitivity analysis. (b) Clustered Saliency map achieved by k -means technique with $k=10$. Note that red areas represent the cluster with the highest saliency. (c) Cortical surface representation with highly salient cortical sources depicted with red dots.

6 Discussion

The present research aims at exploring the interpretability and explainability of the proposed DL-based system in order to provide further insight into the hidden mechanism of cortical sources activation when the brain is preparing hand's open/close movement. To this end, the dataset [35] composed of EEG signals recorded from 15 subjects who performed several repetitions of hand's open and close always starting from a common neutral resting position. EEG recorded during resting (no motion planning) were also analyzed. First, a dataset of EEG epochs of 1s preceding motion onset was constructed. The onset of motion was determined through the signals collected by motion sensors embedded in a glove that the participant had worn throughout the experiment. Beamforming was then applied to EEG epochs to solve the inverse problem and reconstruct the electrical sources in the cortical locations belonging to the primary motor and premotor cortex (i.e., 210 cortical locations, as described in Sect.2.2). Next, such premotor EEG source epochs (1s width) were used as input to a customized deep CNN to perform the following binary

1 classifications: HC vs. RE and HO vs. RE, reporting very good discrimination
2 performance: average accuracy rate up to $89.65 \pm 5.29\%$ and $90.50 \pm 5.35\%$, re-
3 spectively. Hence, the temporal trend of electrical sources in the motor cortex
4 allows in principle for motion planning discrimination from resting phases.
5 However, since the ultimate goal of the present study was to provide an in-
6 depth understanding of which cortical locations contributed the most to the
7 discrimination of HC/HO motion planning from resting phase in the frame of
8 1s preceding the execution of the movement, an occlusion sensitivity analysis
9 was proposed. Specifically, after training and testing the proposed CNN, EEG
10 time-source epochs were systematically occluded with a grey mask and used
11 as input to the pre-trained deep CNN, producing the so called *heatmaps* or
12 *saliency maps*. This technique allows to highlight which areas of the input map
13 (i.e., EEG time-sources epochs) are relevant to the decision making process.
14 In order to detect the high saliency parts in the map, *k*-means clustering was
15 applied and the high-saliency cluster was identified as described in Sect. 5.2.
16 By detecting the high saliency areas in the time-sources maps, the correspond-
17 ing highly relevant source locations could be pinpointed. The more relevant
18 sources were then mapped onto the cortical surface and represented with red
19 dots. As can be seen in Figure 5, a recurring pattern can be detected in
20 each subject. Specifically, the cortical sources located in the central area of
21 the motor cortex (close to the longitudinal fissure) and the temporal zone of
22 the right motor cortex resulted highly relevant during HC/HO movement’s
23 planning preparation. It is to be noted that, to date, it is still not well known
24 whether and how motion planning is spatially organized over the motor cor-
25 tex. A contralateral involvement of the premotor cortex in motion planning
26 was reported in the literature [45] but further details about sub-areas involve-
27 ment are still to be investigated. Hence, our findings may shed a new light
28 on motor preparation and suggest that the aforementioned motor cortical re-
29 gions (i.e., central and temporal right) are the mostly involved in the HC/HO
30 sub-movement preparation. It is also worth noting that intra-subject differ-
31 ences can be observed. For example, in Subjects 01 and 07 (Figure 5), only
32 the right-central sub-region resulted highly relevant to HC detection; whereas,
33 the left-central and also the right-temporal sub-regions look involved in HO
34 detection. To the best of our knowledge, this is the first attempt to study
35 motor preparation through explainable machine learning. Furthermore, this is
36 the first work that attempts to detect the subareas of motor cortex that are
37 more salient to the preparation open/close hand’s movement. Recurrent spa-
38 tial patterns of cortical activation could be detected across subjects, namely,
39 the central area close to the longitudinal fissure and the right temporal area of
40 the premotor and primary motor cortex. However, the proposed methodology
41 has some limitations. First, the number of EEG channels used in this study
42 was 61, we think that using a higher number of electrodes would have a pos-
43 itive impact on inverse problem solution, leading to a more accurate cortical
44 source reconstruction. Second, the number of EEG epochs used to train the
45 proposed CNN was limited. Overall, each class (HC, HO, RE) included only
46 60 EEG epochs. Third, movement’s onset was marked by processing the data
47
48
49
50
51
52
53
54
55
56
57
58
59
60
61
62
63
64
65

1 collected by the motion sensors embedded in the glove that the participant
2 used to wear during the experiment. Motion data collected through the glove
3 are smooth and do not allow to detect onset instantaneously, which means
4 the epochs used for training may have captured the early ms of motion imple-
5 mentation, causing, in principle, the similar activation patterns visible in HC
6 and HO (Figure 5). For the aforementioned reasons, in the future, we intend
7 not only to enroll a larger cohort of subject and record high-density EEGs
8 (128-256 channels) but, for a more precise motion onset detection, EEG will
9 be co-registered with electromyography (EMG).
10

11 **7 Conclusion**

12
13
14 In this paper we proposed a novel deep CNN capable of classifying time-source
15 maps (i.e., EEG sources epochs) related to hands' sub-movements (open/close)
16 phase from resting state, achieving remarkable results, namely, average accu-
17 racy of 89.65 ± 5.29 in HC vs. RE and average accuracy of 90.50 ± 5.35 in HO
18 vs. RE discrimination task. Furthermore, in order to investigate which cortical
19 source has mostly contributed in the classification of hand's motor prepara-
20 tion phase, EML was applied. Occlusion sensitivity analysis allowed to produce
21 suitable *saliency maps*, from which to identify the most relevant areas of the
22 input. The highest saliency region was detected through *k*-means clustering
23 technique and the enclosed cortical sources were mapped onto the cortical
24 surface. Experimental results mainly showed that the central and the right-
25 temporal cortical sub-regions are activating while the subject was planning
26 hand's movements (i.e., HC/HO). It is worth noting that the cortical activa-
27 tion rules that govern the motion planning are still not well known. Hence,
28 on the basis of the achievements here reported, we believe that the proposed
29 approach may be considered to be an interesting breakthrough in BCI appli-
30 cations.
31
32

33 **8 Declarations**

34 **8.1 Funding**

35
36 Not applicable
37

38 **8.2 Conflict of interest**

39
40
41 The authors declare that they have no conflict of interest.
42

43 **8.3 Availability of data and material**

44
45
46 Data are publicly available from the BNCI Horizon 2020 database at <http://bnci-horizon-2020.eu/database/data-sets> (accession number 001-2017).
47
48
49
50
51
52
53
54
55
56
57
58
59
60
61
62
63
64
65

Table 1 Performance of the proposed deep CNN in terms of recall, precision, F1-score and accuracy for the HC vs. RE classification task.

Subject	Recall	Precision	F1-score	Accuracy
S01	86.51±7.76	89.45±11.45	87.36±6.16	87.30±6.58
S02	93.65±5.00	95.92±6.97	94.46±2.00	94.44±2.27
S03	87.30±9.47	91.96±13.10	88.67±7.36	88.49±8.70
S04	92.06±6.30	93.67±7.89	92.48±3.33	92.46±3.48
S05	89.68±8.13	81.42±6.57	84.96±4.00	84.13±4.45
S06	88.10±8.13	90.69±6.58	89.09±5.51	89.29±5.18
S07	80.16±12.77	80.83±12.36	79.86±9.60	79.76±10.11
S08	96.03±4.20	100.00±0.00	97.94±2.21	98.02±2.10
S09	96.83±4.37	98.41±2.73	97.57±3.05	97.62±2.97
S10	96.83±4.37	97.86±5.67	97.25±4.09	97.22±4.24
S11	81.75±14.24	86.29±15.31	82.29±8.76	82.14±10.25
S12	90.48±4.20	91.76±8.15	90.95±5.04	90.87±5.25
S13	87.30±8.91	90.99±9.62	88.72±7.06	88.89±7.17
S14	83.33±5.56	89.37±5.94	86.05±3.50	86.51±3.37
S15	87.14±5.24	89.18±5.87	87.68±2.97	87.65±3.29
Average	89.14±7.24	91.19±7.88	89.69±4.98	89.65±5.29

Table 2 Performance of the proposed deep CNN in terms of recall, precision, F1-score and accuracy for the HO vs. RE classification task.

Subject	Recall	Precision	F1-score	Accuracy
S01	84.13±14.50	96.10±8.13	88.62±8.14	89.68±6.15
S02	92.86±6.18	99.25±1.99	95.82±2.97	96.03±2.71
S03	85.71±16.31	94.24±8.11	88.57±10.49	89.68±7.81
S04	89.68±5.00	100.00±0.00	94.50±2.80	94.84±2.50
S05	92.86±7.67	91.52±9.13	91.83±6.10	91.67±6.42
S06	96.03±4.20	87.63±11.93	91.05±5.50	90.08±6.96
S07	77.78±11.11	80.13±18.01	76.95±5.87	75.79±9.72
S08	94.44±4.54	97.86±5.67	96.00±3.75	96.03±3.88
S09	90.48±8.91	97.74±5.97	93.70±6.11	94.05±5.65
S10	92.06±5.42	97.02±5.73	94.32±3.91	94.44±3.93
S11	76.98±12.18	94.62±9.21	84.04±7.29	85.71±6.09
S12	95.24±5.94	83.83±11.60	88.53±4.83	87.30±5.97
S13	88.89±8.49	94.39±6.71	91.35±5.97	91.67±5.78
S14	95.24±3.83	90.23±7.10	92.42±2.79	92.06±3.37
S15	87.31±6.01	91.03±5.66	88.40±3.32	88.50±3.35
Average	89.31±8.02	93.04±7.66	90.41±5.32	90.50±5.35

8.4 Code availability

Custom code will be available on request to the corresponding author.

References

1. Neucube: A spiking neural network architecture for mapping, learning and understanding of spatio-temporal brain data. *Neural Networks* **52**, 62 – 76 (2014)
2. Bengio, Y.: Practical recommendations for gradient-based training of deep architectures. in: *Neural networks: Tricks of the trade* pp. 437–478 (2012)
3. Brodmann, K.: *Brodmann’s: Localisation in the cerebral cortex*. Springer Science & Business Media ((2007))
4. Catani, M.: A little man of some importance. *Brain* **140**(11), 3055–3061 (2017)
5. Craik, A., He, Y., Contreras-Vidal, J.L.: Deep learning for electroencephalogram (EEG) classification tasks: a review. *Journal of neural engineering* **16**(3), 031001 (2019)
6. Doborjeh, Z.G., Doborjeh, M.G., Kasabov, N.: Attentional bias pattern recognition in spiking neural networks from spatio-temporal EEG data. *Cognitive Computation* **10**(1), 35–48 (2018)
7. Edelman, B.J., Baxter, B., He, B.: EEG source imaging enhances the decoding of complex right-hand motor imagery tasks. *IEEE Transactions on Biomedical Engineering* **63**(1), 4–14 (2015)
8. Fellous, J.M., Sapiro, G., Rossi, A., Mayberg, H.S., Ferrante, M.: Explainable artificial intelligence for neuroscience: Behavioral neurostimulation. *Frontiers in Neuroscience* **13**, 1346 (2019)
9. Gao, F., Huang, T., Sun, J., Wang, J., Hussain, A., Yang, E.: A new algorithm for sar image target recognition based on an improved deep convolutional neural network. *Cognitive Computation* **11**(6), 809–824 (2019)
10. Goshvarpour, A., Goshvarpour, A.: A novel approach for EEG electrode selection in automated emotion recognition based on lagged poincare’s indices and sloreta. *Cognitive Computation* pp. 1–17 (2019)
11. Grech, R., Cassar, T., Muscat, J., Camilleri, K.P., Fabri, S.G., Zervakis, M., Xanthopoulos, P., Sakkalis, V., Vanrumste, B.: Review on solving the inverse problem in EEG source analysis. *Journal of neuroengineering and rehabilitation* **5**(1), 25 (2008)
12. Grosse-Wentrup, M., Liefhold, C., Gramann, K., Buss, M.: Beamforming in noninvasive brain-computer interfaces. *IEEE Transactions on Biomedical Engineering* **56**(4), 1209–1219 (2009)
13. Hallez, H., Vanrumste, B., Grech, R., Muscat, J., De Clercq, W., Vergult, A., D’Asseler, Y., Camilleri, K.P., Fabri, S.G., Van Huffel, S., et al.: Review on solving the forward problem in EEG source analysis. *Journal of neuroengineering and rehabilitation* **4**(1), 46 (2007)
14. Haufe, S., Ewald, A.: A simulation framework for benchmarking EEG-based brain connectivity estimation methodologies. *Brain topography* pp. 1–18 (2016)
15. Haufe, S., Huang, Y., Parra, L.C.: A highly detailed FEM volume conductor model based on the ICBM152 average head template for EEG source imaging and TCS targeting. In: *Conf Proc IEEE Eng Med Biol Soc* (2015)
16. Hermes, D., Vansteensel, M.J., Albers, A.M., Bleichner, M.G., Benedictus, M.R., Orellana, C.M., Aarnoutse, E., Ramsey, N.: Functional MRI-based identification of brain areas involved in motor imagery for implantable brain-computer interfaces. *Journal of Neural Engineering* **8**(2), 025007 (2011)
17. Ieracitano, C., Mammone, N., Bramanti, A., Hussain, A., Morabito, F.C.: A convolutional neural network approach for classification of dementia stages based on 2d-spectral representation of EEG recordings. *Neurocomputing* **323**, 96–107 (2019)
18. Ieracitano, C., Mammone, N., Hussain, A., Morabito, F.C.: A novel multi-modal machine learning based approach for automatic classification of EEG recordings in dementia. *Neural Networks* **123**, 176–190 (2020)
19. Kantak, S.S., Stinear, J.W., Buch, E.R., Cohen, L.G.: Rewiring the brain: potential role of the premotor cortex in motor control, learning, and recovery of function following brain injury. *Neurorehabilitation and neural repair* **26**(3), 282–292 (2012)
20. Kingma, D.P., Ba, J.: Adam: A method for stochastic optimization. *arXiv preprint arXiv:1412.6980* (2014)
21. Krizhevsky, A., Sutskever, I., Hinton, G.E.: Imagenet classification with deep convolutional neural networks. In: *Advances in neural information processing systems*, pp. 1097–1105 (2012)

22. Lancaster, J.L., Tordesillas-Gutiérrez, D., Martinez, M., Salinas, F., Evans, A., Zilles, K., Mazziotta, J.C., Fox, P.T.: Bias between MNI and TALAIRACH coordinates analyzed using the ICBM-152 brain template. *Human brain mapping* **28**(11), 1194–1205 (2007)
23. LeCun, Y., Bengio, Y., Hinton, G.: Deep learning. *nature* **521**(7553), 436 (2015)
24. Liang, Z., Shao, J., Zhang, D., Gao, L.: Traffic sign detection and recognition based on pyramidal convolutional networks. *Neural Computing and Applications* pp. 1–11 (2019)
25. Liu, L., Chen, S., Zhang, F., Wu, F.X., Pan, Y., Wang, J.: Deep convolutional neural network for automatically segmenting acute ischemic stroke lesion in multi-modality mri. *Neural Computing and Applications* pp. 1–14 (2019)
26. Lotte, F., Bougrain, L., Cichocki, A., Clerc, M., Congedo, M., Rakotomamonjy, A., Yger, F.: A review of classification algorithms for EEG-based brain–computer interfaces: a 10 year update. *Journal of Neural Engineering* **15**(3), 031005 (2018)
27. Lotte, F., Jeunet, C.: Online classification accuracy is a poor metric to study mental imagery-based BCI user learning: an experimental demonstration and new metrics. In: 7th International BCI Conference, pp. hal-01519478 (2017)
28. Malmivuo, J., Plonsey, R.: *Bioelectromagnetism, Principles and Applications of Bioelectric and Biomagnetic Fields*. New York, Oxford, Oxford University Press (1995)
29. Mammone, N., Ieracitano, C., Morabito, F.C.: A deep cnn approach to decode motor preparation of upper limbs from time–frequency maps of EEG signals at source level. *Neural Networks* **124**, 357–372 (2020)
30. Mammone, N., Morabito, F.C.: Enhanced Automatic Wavelet Independent Component Analysis for Electroencephalographic Artifact Removal. *Entropy* **16**(12), 6553–6572 (2014)
31. Montavon, G., Samek, W., Müller, K.R.: Methods for interpreting and understanding deep neural networks. *Digital Signal Processing* **73**, 1–15 (2018)
32. Müller-Putz, G.R., Schwarz, A., Pereira, J., Ofner, P.: From classic motor imagery to complex movement intention decoding: The noninvasive Graz-BCI approach. In: *Progress in brain research*, vol. 228, pp. 39–70. Elsevier (2016)
33. Nair, V., Hinton, G.E.: Rectified linear units improve restricted boltzmann machines. In: *Proceedings of the 27th international conference on machine learning (ICML-10)*, pp. 807–814 (2010)
34. Nunez, P.L., Srinivasan, R.: *Electric fields of the brain, The neurophysics of EEG*. New York, Oxford University Press (2006)
35. Ofner, P., Schwarz, A., Pereira, J., Müller-Putz, G.R.: Upper limb movements can be decoded from the time-domain of low-frequency EEG. *PloS one* **12**(8), e0182578 (2017)
36. Ofner, P., Schwarz, A., Pereira, J., Wyss, D., Wildburger, R., Müller-Putz, G.R.: Attempted arm and hand movements can be decoded from low-frequency EEG from persons with spinal cord injury. *Scientific reports* **9**(1), 7134 (2019)
37. Powers, D.M.: Evaluation: from precision, recall and f-measure to roc, informedness, markedness and correlation. *Journal of Machine Learning Technologies* **2**(1), 37–63 (2011)
38. Roy, Y., Banville, H., Albuquerque, I., Gramfort, A., Falk, T.H., Faubert, J.: Deep learning-based electroencephalography analysis: a systematic review. *Journal of neural engineering* **16**(5), 051001 (2019)
39. Scherer, D., Müller, A., Behnke, S.: Evaluation of pooling operations in convolutional architectures for object recognition. In: *International conference on artificial neural networks*, pp. 92–101. Springer (2010)
40. Shakeel, A., Navid, M.S., Anwar, M.N., Mazhar, S., Jochumsen, M., Niazi, I.K.: A review of techniques for detection of movement intention using movement-related cortical potentials. *Computational and mathematical methods in medicine* p. 346217 (2015)
41. Tadel, F., Baillet, S., Mosher, J.C., Pantazis, D., Leahy, R.M.: Brainstorm: a user-friendly application for MEG/EEG analysis. *Computational intelligence and neuroscience* p. 8 (2011)
42. Tang, W., Zou, D., Yang, S., Shi, J., Dan, J., Song, G.: A two-stage approach for automatic liver segmentation with faster r-cnn and deeplab. *Neural Computing and Applications* pp. 1–10 (2020)
43. Vecchiato, G., Del Vecchio, M., Ascari, L., Antopolskiy, S., Deon, F., Kubin, L., Ambeck-Madsen, J., Rizzolatti, G., Avanzini, P.: Electroencephalographic time-frequency patterns of braking and acceleration movement preparation in car driving simulation. *Brain research* **1716**, 16–26 (2019)

- 1 44. Wagstaff, K., Cardie, C., Rogers, S., Schrödl, S., et al.: Constrained k-means clustering
2 with background knowledge. In: *Icml*, vol. 1, pp. 577–584 (2001)
- 3 45. Zama, T., Shimada, S.: Simultaneous measurement of electroencephalography and near-
4 infrared spectroscopy during voluntary motor preparation. *Scientific reports* **5**(1), 1–9
5 (2015)
- 6 46. Zeiler, M.D., Fergus, R.: Visualizing and understanding convolutional networks. In:
7 European conference on computer vision, pp. 818–833. Springer (2014)
- 8 47. Zeng, H., Song, A.: Optimizing single-trial EEG classification by stationary matrix
9 logistic regression in brain–computer interface. *IEEE transactions on neural networks
10 and learning systems* **27**(11), 2301–2313 (2016)

11
12
13
14
15
16
17
18
19
20
21
22
23
24
25
26
27
28
29
30
31
32
33
34
35
36
37
38
39
40
41
42
43
44
45
46
47
48
49
50
51
52
53
54
55
56
57
58
59
60
61
62
63
64
65

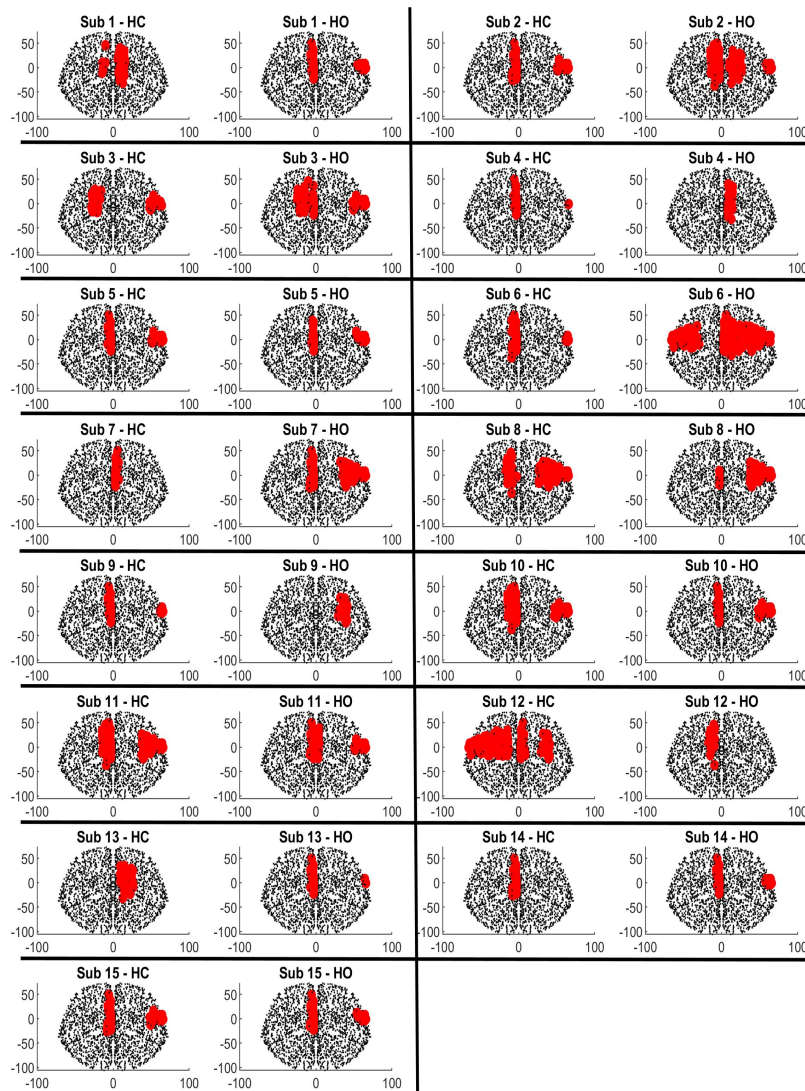


Fig. 5 Cortical surface representations of each subject. Red dots indicate the highly salient cortical sources locations that have mostly involved in the prediction task (i.e. HC/HO).